Applied Catalysis B: Environmental 218 (2017) 731–742

Contents lists available at ScienceDirect

Applied Catalysis B: Environmental

journal homepage: www.elsevier.com/locate/apcatb

Relationship between structures and activities of supported metal vanadates for the selective catalytic reduction of NO by NH_3

Adrian Marberger[a,b], Davide Ferri[a], Martin Elsener[a], Amod Sagar[c], Christine Artner[c], Karl Schermanz[c], Oliver Kröcher[a,b,*]

[a] Paul Scherrer Institut, CH-5232 Villigen PSI, Switzerland
[b] École Polytechnique Fédérale de Lausanne (EPFL), Institute of Chemical Science and Engineering, CH-1015 Lausanne, Switzerland
[c] Department of Chemistry R&D, Treibacher Industrie AG, A-9330 Althofen, Austria

ARTICLE INFO

Article history:
Received 15 March 2017
Received in revised form 31 May 2017
Accepted 20 June 2017
Available online 1 July 2017

Keywords:
SCR
Vanadates
Diffuse reflectance spectroscopy
VO_x
Decomposition

ABSTRACT

Transition and rare earth metal vanadates are potential active phases for the selective catalytic reduction (SCR) of nitric oxide by ammonia for exhaust gas emission control. In this work, various metal vanadates mixed with SiO_2-WO_3-TiO_2 (TWS) were compared to vanadia-based SCR catalysts. $FeVO_4$-based catalysts were found to be the most active metal vanadates, followed by $CeVO_4$ and $ErVO_4$. In depth analysis using XRD, BET, H_2-TPR, DRUV and DRIFTS demonstrated that the vanadates partly decomposed above 600–750 °C to the corresponding single metal oxides, the decomposition temperature correlating with their relative stability. The activity and the estimated fraction of freed VO_x from the vanadate decomposition strongly correlated with vanadia-based catalysts at comparable V-loading. Based on these findings, the enhanced thermal stability of the vanadate-based catalysts was correlated to an overall lower amount of free VO_x species compared to vanadia-based catalysts. The released VO_x species are responsible for the activity of the metal vanadate-based SCR catalysts and are of similar nature to those of vanadia-based catalysts. Therefore, the claimed high temperature stability advantage of supported metal vanadates is merely an effect of the degree of vanadate decomposition and is not related to their intrinsic stability.

1. Introduction

Efficient removal of nitric oxides (NO_x) from exhaust gases of diesel engines is realized by reacting NH_3 on a solid catalyst according to the standard selective catalytic reduction (SCR) scheme (Eq. (1)) [1,2].

$$4NO + 4NH_3 + O_2 \rightarrow 4N_2 + 6H_2O \quad (1)$$

The catalyst is typically composed of dispersed VO_x species on a (silica)-tungsta-titania support (herein labelled as V_2O_5-based catalyst for simplicity). The catalyst activity and stability are dependent on the V loading and generally decrease after exposure to temperatures above 650 °C [3,4]. Due to the increasingly stringent automotive emission regulations, the SCR technology started to be attractive in the automotive sector as well in order to control the NO_x emissions of passenger vehicles. However, this has generated concerns on the thermal stability of V_2O_5-based catalysts because of V volatility and fostered research on high temperature stable SCR catalysts. To this end, metal vanadates ($MeVO_4$) were proposed as potential candidates as an active phase substitute of V_2O_5-based SCR catalysts. One advantage of $MeVO_4$ is the higher melting point (e.g. 850 °C [5] and 1100 °C [6] for $FeVO_4$ and $CeVO_4$, respectively) compared to V_2O_5, which becomes mobile already above 690 °C. It has been reported that $MeVO_4$ exhibit excellent resistance to deactivation after impregnation on SiO_2-WO_3-TiO_2 (TWS) and remain active after severe aging [7,8]. In view of stability requirements against temperature surges, it is beneficial to use TWS due to the increase in structural strength [9–12].

The enhanced thermal stability of catalysts based on rare earth vanadates supported on TWS is associated mainly with the ability of the rare earth metals to suppress the undesired anatase to rutile phase transition of the support. This consequently hinders the sintering and shifts the loss of surface area to higher calcination temperatures. Since vanadium is locked in the vanadate structure, no free V_2O_5 that would promote sintering is dispersed on the catalyst surface [7]. Except for $LaVO_4$, a broad range of rare earth vanadate based SCR catalysts exhibit high thermal stability. Especially $ErVO_4$ and $TbVO_4$ were found the most active and temperature stable compositions [7,8]. However, the catalysts were

* Corresponding author at: Paul Scherrer Institut, CH-5232 Villigen PSI, Switzerland.
E-mail address: oliver.kroecher@psi.ch (O. Kröcher).

http://dx.doi.org/10.1016/j.apcatb.2017.06.061
0926-3373/

previously compared with a V_2O_5-based one whose high loading is not suitable for high temperature treatment [4]. The best compromise between low-temperature activity and thermal stability was found for mixed $Fe_{0.5}Er_{0.5}VO_4$/TWS [13], which was interpreted to originate from both Fe and Er, the former promoting the low temperature activity because of the $FeVO_4$ decomposition to Fe_2O_3 and VO_x species and the latter increasing the structural stability of the system.

Cerium is widely considered as SCR active component due to its redox ability and promotional effects such as increased acidity and enhanced oxygen storage capacity. The redox properties of the Ce^{4+}/Ce^{3+} pair and the propensity of Ce to form solid solutions with other oxides thus increasing the amount of active sites and improving the (hydro)-thermal stability represent relevant benefits of CeO_2 [14–21]. Ce-modified V_2O_5-based SCR catalysts showed enhanced thermal stability because the formation of cerium vanadate decreased sintering tendencies [22]. Supported rare earth vanadate catalysts, among which $CeVO_4$, were found to be more thermally stable compared to a V_2O_5-based reference catalyst [7,8]. Finally, it was shown that unsupported $CeVO_4$ and transition metal vanadates can exhibit some SCR activity [23–25].

Supported $FeVO_4$ was also reported to be advantageous with respect to aging, selectivity and low temperature SCR activity compared to V_2O_5-based catalysts [26–29]. Liu et al. [30] prepared $FeVO_4$ from co-impregnation of Fe and V precursors directly on TiO_2. After calcination below 600 °C, 9 wt% $FeVO_4/TiO_2$ showed excellent NO_x conversion. However, a severe NH_3–SCR activity loss was observed for calcination at higher temperature. The deactivation was associated with the loss of surface area resulting from the phase transformation of TiO_2. We have recently shown that supported $FeVO_4$ obtained from mixing $FeVO_4$ and TWS is not stable and decomposes into Fe_2O_3 and VO_x species above 600 °C [31]. Below this temperature, the intrinsic activity of $FeVO_4$-based SCR catalysts was rather low and was only enhanced by its thermal decomposition into VO_x species. We showed using XANES that these species resembled those obtained on classic V_2O_5-based SCR catalysts [26,31]. The decomposition of the vanadate could be used as an argument to justify many of the observations reported above for rare earth vanadates and $FeVO_4$. Hence, in order to clarify the benefits of $MeVO_4$ on TWS, in this work we compare the activity and stability of $FeVO_4$, $CeVO_4$ and $ErVO_4$ on TWS, aiming at unraveling the origin of their controversial SCR activity.

2. Experimental

The bulk metal vanadates ($CeVO_4$, $FeVO_4$, $ErVO_4$, Table S1) were provided by Treibacher Industrie AG and were obtained from co-precipitation of metals and vanadium precursors. The powders were dried at 120 °C and calcined at 700 °C if needed. TiO_2-WO_3-SiO_2 (TWS, Tiona DT-58, 10 wt% SiO_2, 9 wt% WO_3, and 81 wt% TiO_2, Cristal Global) was used as the catalyst support. After mixing $CeVO_4$, $FeVO_4$, $ErVO_4$, CeO_2 (Sigma-Aldrich) or ammonium vanadate (NH_4VO_3, Sigma-Aldrich) with TWS in 5 eq. of H_2O at RT for 1 h (V content according to Tables 1 and 2), the slurry was sonicated for 10 min, homogenized with a disperser (30,000 rpm, 5 min) and stirred at 50 °C for 30 min. The solvent was removed under reduced pressure and the resulting powder was dried at 120 °C and calcined at 450 °C for 3 h in a muffle oven. For the sake of comparison, the metal vanadate loading was based on the amount of nominal V_2O_5, e.g. 5.6 wt% $CeVO_4$-TWS is equivalent to 2.0 wt% V_2O_5. For the coating of the cordierite monoliths, a washcoat was prepared by mixing the catalyst powder with 3 eq. of H_2O followed by homogenization and ultrasonication. The honeycomb monoliths (cordierite, 400 cpsi, ca. 12 mm × 17 mm × 50 mm) were coated by repeated immersion and drying until the desired catalyst loading was reached (1.30 g, ca. 125 g/L). The washcoated monoliths (estimated washcoat thickness of ca. 20–40 μm) were calcined in air at 450 °C for 10 h. The slurry left over from the washcoating process was dried and the obtained powder was calcined in air at 450 °C for 10 h. These samples were then subjected to the characterization as mentioned below. Calcination of powders and monoliths was carried out in a muffle oven at 650, 700, 750 and 800 °C for 10 h. The catalysts composition, V content and abbreviations are summarized in Tables 1 and 2.

2.1. Catalytic measurements

The washcoated monoliths were tested on a dedicated laboratory test reactor [32,33] using a feed of 10 vol% O_2, 5 vol% H_2O, 500 ppm NO, 0–600 ppm NH_3 with balance N_2 (total gas flow ca. 500 L/h) in order to mimic realistic exhaust gas composition. The dosage of NH_3 was varied to determine the NO reduction efficiency at 10 ppm NH_3 slip [33]. The gas hourly space velocity (GHSV = volumetric gas flow/coated monolith volume) was 50,000 h^{-1}, which is typical for SCR converters of diesel vehicles [34]. The maximum NO_x reduction activity was measured by dosing excess NH_3, i.e. at $NH_3/NO_x = 1.2$ [3]. Under the assumption of a zeroth kinetic order with respect to NH_3 and pseudo-first order with respect to NO, the mass specific rate constant (k_{mass}) for the maximum NO reduction efficiency was calculated according to Eq. (2) [35,36],

$$k_{mass} = \frac{V*}{A} \cdot \ln\left(1 - X_{NO_x}\right) \quad (2)$$

where V^* is the total flow rate at reaction conditions, A the loading of the active component and X_{NOx} the fractional NO_x conversion. Despite the adsorption of both NH_3 and NO at low temperature, the first order SCR reaction with respect to NO is justified because NH_3 adsorption dominates on acidic SCR catalysts [2]. The independence of the rate constant from the loading is essential for washcoated monoliths where small loading deviations are unavoidable. The NO_x reduction efficiency (DeNOx) was calculated according to Eq. (3) [35,37],

$$\mathrm{DeNO}x = \frac{C^{in}_{NO} - C^{out}_{NO_x} C^{in}_{NO}}{} \cdot 100\% \quad (3)$$

where $C^{in}{}_{NO}$ is the NO concentration upstream of the catalyst and $C^{out}{}_{NOx}$ the NO and NO_2 concentrations downstream of the catalyst. A calibrated FT-IR spectrometer (Nexus Thermo Fisher) equipped with a heated gas cell was used for the online gas analysis of the exhaust gas.

2.2. Characterization methods

Powder X-ray diffraction (XRD) patterns were measured on a D8 ADVANCE (Bruker) diffractometer using Cu Kα1 radiation (λ = 1.5406 Å), a primary slit (0.3°) and a Ni filter in the secondary beam path. The phases were identified with the X'Pert HighScore Plus software. Data were recorded in the 2Θ range 15–60° using a step size of 0.03° and an acquisition time of 2 s. The crystallite size of anatase TiO_2 was determined from the Scherrer equation using the reflections at 25.4 and 48.0°. The BET specific surface area (SSA) was measured by N_2 adsorption at −196 °C on a Quantachrome Autosorb I instrument. Prior to the measurement, the samples were outgassed at 350 °C for 3 h. Temperature programmed reduction with H_2 (H_2-TPR) was conducted on a bench top TPDRO-1100 (ThermoElectron) instrument equipped with a thermal conductivity detector. The calcined powder samples (ca. 100 mg) were loaded into the quartz reactor tube and heated under constant flow of 20 vol% O_2 to 500 °C. After cooling to room temperature, H_2-TPR profiles were recorded in 10 vol% H_2/Ar (20 mL/min) at

Table 1
Nominal V_2O_5 content, estimated $r(V_2O_5)$, TiO_2 crystallite size, k_{mass}, BET surface area, calculated V surface coverage (ξ) of FeV-TWS, CeV-TWS and ErV-TWS after calcination at 750 °C.

	Me	$MeVO_4$ loading (wt%)	Nominal V_2O_5 (wt%)[a]	After calcination at 750 °C for 10 h				
				Released V_2O_5 (wt%)[b]	TiO_2 size (nm)[b]	k_{mass} ($cm^3\ g^{-1}\ s^{-1}$)	BET SSA ($m^2\ g^{-1}$)	ξ (%)[c]
4CeV-TWS	Ce	4.2	1.5	0.6 ± 0.1	20	71	71	7
6CeV-TWS	Ce	5.6	2.0	0.7 ± 0.1	19	79	69	9
7CeV-TWS	Ce	7.0	2.5	0.8 ± 0.2	20	101	69	10
9CeV-TWS	Ce	9.1	3.3	1.1 ± 0.2	19	123	67	14
11CeV-TWS	Ce	11.2	4.0	1.2 ± 0.2	23	141	53	20
4FeV-TWS	Fe	3.75	2.0	2.0	26	299	49	34
5FeV-TWS	Fe	5.0	2.7	2.7	36	198	33	69
6ErV-TWS	Er	6.1	2.0	0.2 ± 0.2	21	30	70	2
10ErV-TWS	Er	10	3.3	0.1 ± 0.3	19	33	69	1
6CeV-dried-TWS	Ce[d]	5.6	2.0	1.1 ± 0.1	25	137	57	16

[a] Based on V_2O_5 equivalents.
[b] Estimated from XRD.
[c] Determined from theoretical saturation value (7.9 $VO_x\ nm^{-2}$ [44]) for monolayer coverage and the BET surface area.
[d] $CeVO_4$ dried at 120 °C.

Table 2
TiO_2 crystallite size, k_{mass}, BET surface area, calculated V surface coverage (ξ) of V_2O_5-based catalysts after calcination at 750 °C.

	V_2O_5 loading (wt%)	TiO_2 size (nm)[a]	k_{mass} ($cm^3\ g^{-1}\ s^{-1}$)	BET SSA ($m^2\ g^{-1}$)	ξ (%)[b]
0V-TWS	0	20	10	78	0
0.5V-TWS	0.5	19	67	72	6
1V-TWS	1	21	148	61	14
2V-TWS	2	55	198	21	80

[a] Estimated from XRD in Fig. S3.
[b] Determined from theoretical saturation value (7.9 $VO_x\ nm^{-2}$) [44] for monolayer coverage and the BET surface area.

5 °C/min. Diffuse reflectance Fourier transform infrared (DRIFT) spectra were measured using a Bruker Vertex 70 spectrometer (Bruker) equipped with a liquid N_2 cooled MCT detector and a Praying Mantis mirror unit (Harrick). The homemade DRIFT cell was equipped with a flat CaF_2 window (d = 25 mm; 2 mm thick) and was connected to gas supply lines. The catalyst powder was finely ground and softly pressed in the sample holder of the cell. Prior to the experiments, the samples were dried in situ in 10 vol% O_2 (100 mL/min, bal. N_2) at 400 °C for 1 h. After cooling to 250 °C, a background spectrum was collected prior to admittance of NH_3. NH_3 adsorption was followed during exposure to 500 ppm of NH_3 + 5 vol% O_2 flow (100 mL/min, bal. N_2) at 250 °C for 15 min. All spectra were collected by accumulating 100 scans at 4 cm^{-1} resolution and a scanner velocity of 80 kHz. The diffuse reflectance ultraviolet visible (DRUV) spectra were measured using a Carry 4000 spectrometer (Agilent) equipped with the same set of mirrors used for DRIFT. The spectra were recorded in the range 200–800 nm and are presented in Kubelka-Munk units [38], $F(R) = (1-R)^2/2R$, where R is the absolute reflectance of the sampled layer. All TWS containing samples were background corrected using a spectrum of TWS calcined at 450 °C, while $BaSO_4$ was used as background for all reference samples. The Fityk software [39] was exploited for the deconvolution of the DRIFT and DRUV data using Gaussian functions for all features.

3. Results and discussion

3.1. Catalytic activity

The NO reduction efficiency of 5.6 wt% $CeVO_4$-TWS (6CeV-TWS, equivalent to 2.0 wt% V_2O_5, Table 1) and 9.1 wt% $CeVO_4$-TWS (9CeV-TWS, 3.3 wt% V_2O_5) calcined at various temperatures is presented in Fig. 1a and b, respectively. The activity of samples calcined at 450 °C (hereafter defined as the fresh state) and at 650 °C was similar and rather modest (maximum at 450–500 °C with ca. 80% conversion). The intrinsic activity of CeV-TWS is evident after comparison with the activity of TWS (Fig. 2b). Especially for 9CeV-TWS, the NO reduction efficiency increased after calcination at 700 and 750 °C and 90% conversion was obtained. This effect is more clearly visible in the k_{mass} values obtained at the reaction temperature of 300 °C (Fig. 1c) showing that calcination at 700 and 750 °C resulted in higher reaction rates. The k_{mass} values of fresh 6CeV-TWS and 9CeV-TWS were comparable, but the k_{mass} of 9CeV-TWS was nearly twice that of 6CeV-TWS after calcination at 700 °C and at 750 °C. The NO reduction efficiency declined above 400 °C for both catalysts after calcination at 800 °C signifying the propensity of the material towards thermal aging and selectivity loss that can be verified by the characterization data presented below. Because the highest NO reduction efficiency was obtained after calcination at 750 °C, the effect of $CeVO_4$ loading was studied with catalysts calcined at this temperature (Fig. 2). The loading of 9 wt% $CeVO_4$ was found to be optimal and a maximum of ca. 90% NO reduction efficiency was reached between 350 °C and 450 °C (Fig. 2a). The overall SCR activity of the $CeVO_4$-based catalysts and their corresponding k_{mass} values (Table 1) were rather low compared to those of a $FeVO_4$ catalyst based on the same TWS support [31]. In view of the further discussion, the activity of CeV-TWS was also compared with that of a vanadia and CeO_2-based catalyst (Fig. 2b). The activity for the vanadia-based reference catalysts increased with increasing V content from 0.0 wt% V_2O_5 (0V-TWS) to 0.5 wt% V_2O_5/TWS (0.5V-TWS) and to 1.0 wt% V_2O_5/TWS (1V-TWS) after calcination at 750 °C. For a V_2O_5 loading of 2 wt% (2V-TWS), the catalyst showed similar activity for all calcination temperatures (Fig. S1) but deactivated after calcination at 750 °C (drop of NO conversion above 400 °C and maximum NO conversion of 80%). A lower V content causes an activity decrease of V_2O_5-WO_3-TiO_2 catalysts (no SiO_2) but also an increase in their thermal stability [3]. Therefore, a compromise between V content and calcination temperature is a requirement for active and stable V_2O_5-based catalysts. 9CeV-TWS was at best as active as 1V-TWS calcined at 750 °C (Fig. 2a and b) but was more active than 2V-TWS calcined at 750 °C. This deactivation was attributed

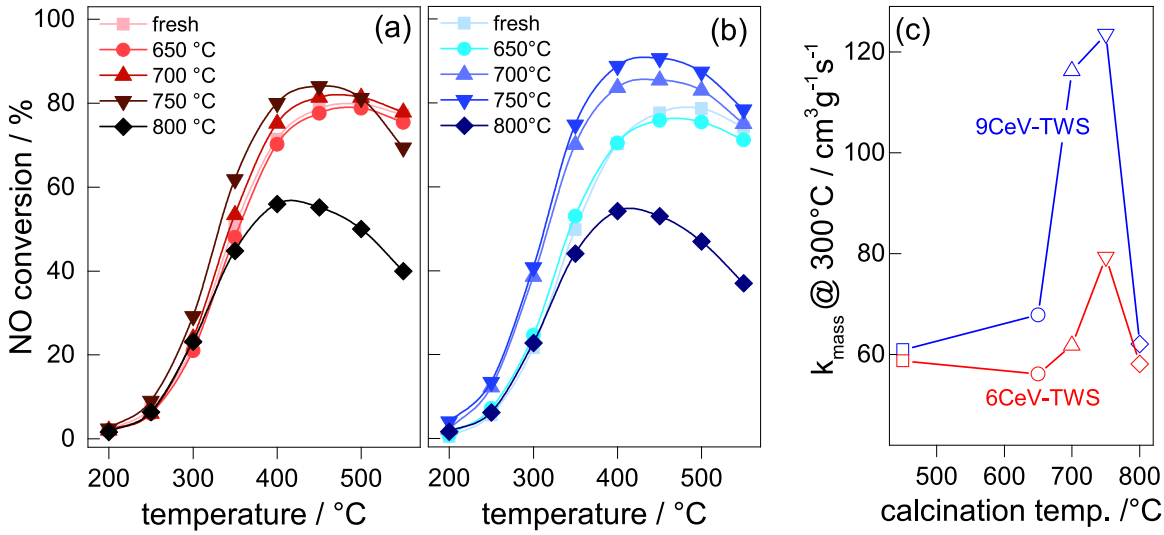

Fig. 1. SCR activity of (a) 6CeV-TWS, (b) 9CeV-TWS calcined at various temperatures and (c) the corresponding mass normalized rate constants k_{mass}.

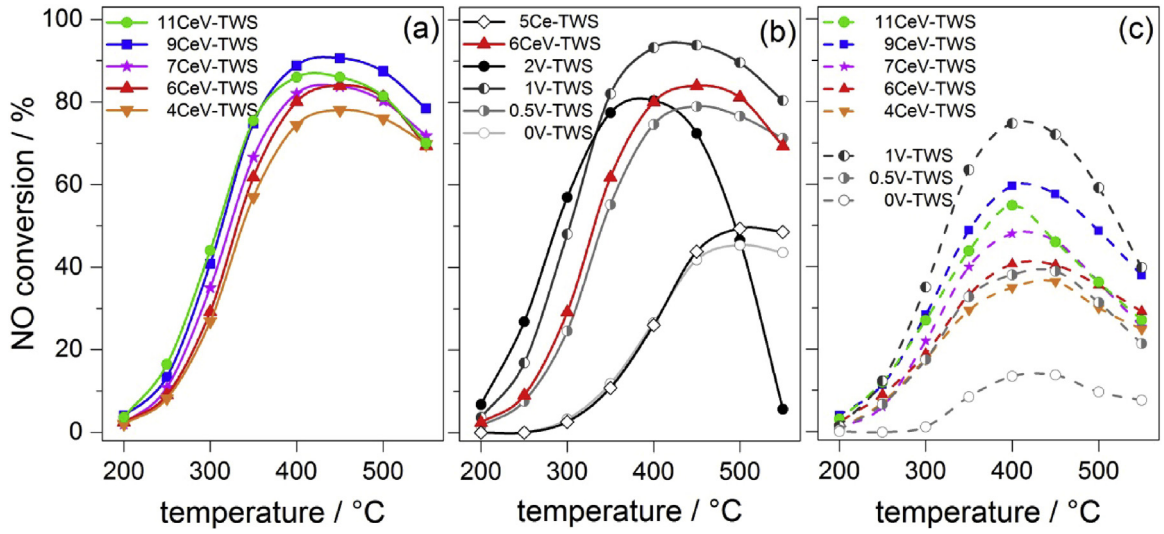

Fig. 2. SCR activity of (a) $CeVO_4$-based catalysts and (b) reference V_2O_5 and CeO_2-based catalysts. (c) Corresponding SCR activity at 10 ppm NH_3 slip. All materials were calcined at 750 °C for 10 h.

to the lower N_2 selectivity caused by an increased NH_3 oxidation activity (Fig. S2). Following the analogy with V-TWS, the NO reduction efficiency of 6CeV-TWS was between that of 0.5V-TWS and 1V-TWS (Fig. 2b). No significant aging tendencies were observed for 6CeV-TWS after calcination at 750 °C. Increasing the loading of $CeVO_4$ to 11 wt% (11CeV-TWS, 4.0 wt% V_2O_5) was no longer beneficial for the activity. Finally, the activity of 9CeV-TWS calcined at 750 °C was not dictated by the CeO_2 possibly present because of the high calcination temperature as demonstrated with 5.0 wt% CeO_2-TWS (5Ce-TWS, equimolar amount of Ce as 9CeV-TWS; Fig. 2b). The reason to select CeO_2 will become clear with the characterization data.

The NO reduction efficiency at 10 ppm NH_3 slip (Fig. 2c) delivers additional useful information since it is a qualitative indication of surface acidity deviations, e.g. upon sintering of the support or poisoning of acid sites [33]. A high surface acidity is beneficial for the NH_3 storage property and delays the NH_3 slip [3,31]. In Fig. 2c, this parameter was lower in all CeV-TWS catalysts compared to that of 1V-TWS, despite the overall higher equivalent V content (Table 1). This indicates that the acidity of CeV-TWS was lower than that of the V_2O_5-based catalyst and the catalyst was not able to store the needed amount of NH_3 for the reaction. After calcination at 750 °C, the CeV-TWS catalysts exhibited higher NO reduction efficiency above 400 °C than 2V-TWS, indicating a lower deactivation effect (lower competing NH_3 oxidation reaction, Fig. S2). This high activity and the increased thermal stability have been interpreted previously as the intrinsic properties of rare earth metal vanadates and the result of a stabilization effect of the support by the vanadate [7,8]. Hence, we have studied the origin of the activity and resistance to deactivation of $MeVO_4$ based SCR catalysts using X-ray powder diffraction (XRD), ex situ diffuse reflectance ultra-violet visible spectroscopy (DRUV) and in situ diffuse reflectance infrared Fourier transform spectroscopy (DRIFT).

3.2. Material characterization

3.2.1. X-ray diffraction

Fig. 3a shows the X-ray diffractograms of 6CeV-TWS calcined at increasing temperature, unsupported $CeVO_4$ calcined at 700 °C and 750 °C and TWS calcined at 750 °C. The prominent TiO_2 anatase reflections were visible in all TWS-containing samples. The anatase TiO_2 crystallite size increased with increasing calcination temper-

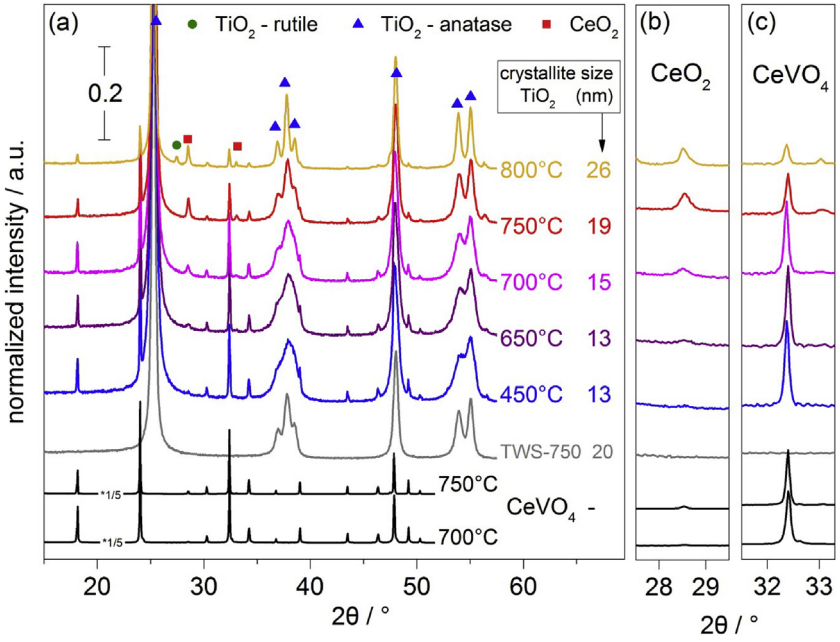

Fig. 3. (a) XRD patterns of unsupported $CeVO_4$, TWS and 6CeV-TWS calcined at various temperatures. TiO_2 anatase crystallite sizes were determined from the Scherrer equation. The 2θ regions (b) around 28.5° ($CeVO_4$) and (c) 32.4° (CeO_2) are enlarged.

ature but was similar for TWS (20 nm) and 6CeV-TWS (19 nm) after calcination at 750 °C indicating that indeed $CeVO_4$ did not promote sintering. While the main peak of $CeVO_4$ at 32.4° (Fig. 3c) decreased with increasing calcination temperature, the reflection at 28.6° (Fig. 3b) assigned to CeO_2 appeared clearly at 650 °C and intensified with increasing calcination temperature.

The XRD data suggests that supported $CeVO_4$ is not as stable as unsupported $CeVO_4$ and decomposed in analogy to our previous findings with supported $FeVO_4$ [31]. CeO_2 was the only visible decomposition product from the $CeVO_4$ phase. The corresponding amount of vanadium made available by $CeVO_4$ decomposition did not form a phase that was detectable by XRD, suggesting that the amount of V was low and/or that the new V-containing phase was highly dispersed. The fraction of released VO_x species was estimated from the peak area of the $CeVO_4$ reflection at 32.4°:

$$r(V_2O_5) = n(V_2O_5) * \left(1 - \frac{A_{CeVO_4(x°C)}}{A_{CeV-TWS(450°C)}}\right) \quad (4)$$

where $r(V_2O_5)$ is the released fraction of VO_x species expressed in wt% V_2O_5, $n(V_2O_5)$ the equivalent V_2O_5 content (in wt%) for each catalyst according to Tables 1 and 2, $A_{CeVO4(x°C)}$ the $CeVO_4$ peak integral area in the diffractograms obtained at the selected calcination temperature x, and $A_{CeVO4(450\,°C)}$ the same integral area for the fresh sample in which $CeVO_4$ is still intact (taken as 100%). This assumption is valid because the areas of the $CeVO_4$ and CeO_2 reflections were similar at 450 and 650 °C, indicating that the metal vanadate remained unchanged after calcination at 450 °C. The error on $r(V_2O_5)$ was calculated by including the peak area of $CeVO_4$ at 18.1° as an additional measurement as well as an integration error (10%). Differences in structure and coordination of the released VO_x species could not be distinguished with this estimation and were investigated by diffuse reflectance spectroscopy in the sections below. It is important to note that $r(V_2O_5)$ does not necessarily reflect the accurate amount of free VO_x. Since small $CeVO_4$ crystallites below the detection limit of XRD, amorphous $CeVO_4$ phases or decomposed $CeVO_4$ during the washcoating procedure are not included, $r(V_2O_5)$ is only an estimate for the sake of our discussion. We also assume here that the extent of vanadium loss due to volatilization is negligible by using TWS (ca. 50 ng/g V_2O_5 for 2 wt% V_2O_5-TWS calcined at 750 °C) [40].

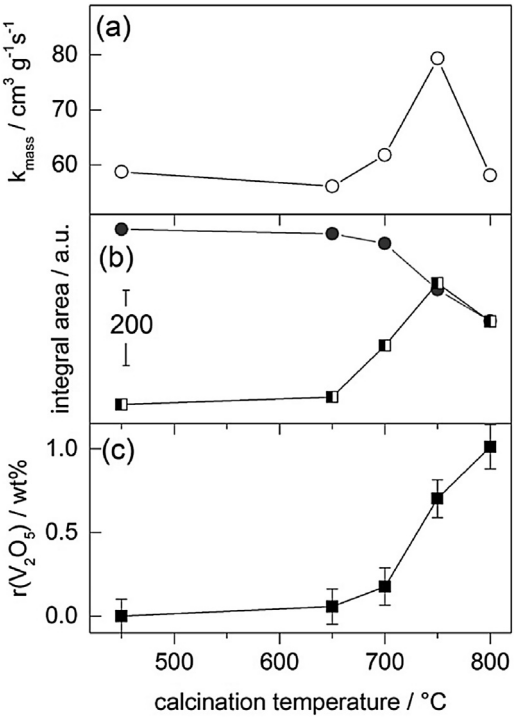

Fig. 4. (a) k_{mass} values obtained at 300 °C for 6CeV-TWS calcined at the indicated temperatures. (b) XRD peak integral areas of 6CeV-TWS ((●) $CeVO_4$, 32.4°; (◧) CeO_2, 28.6°). (c) Released VO_x (calculated and displayed as V_2O_5 ($r(V_2O_5)$)).

Fig. 4 shows the calcination temperature dependence of the structural changes of 6CeV-TWS expressed in terms of the integral areas of the $CeVO_4$ and CeO_2 peaks (Fig. 4b, data from Fig. 3b and c), of the corresponding $r(V_2O_5)$ (Fig. 4c, Eq. (4)) and of the catalytic performance expressed in terms of k_{mass} (Fig. 4a, data from Fig. 1a). The appearance of the CeO_2 reflections, the decrease of those of $CeVO_4$ and the increase of the k_{mass} after calcination at 700 °C

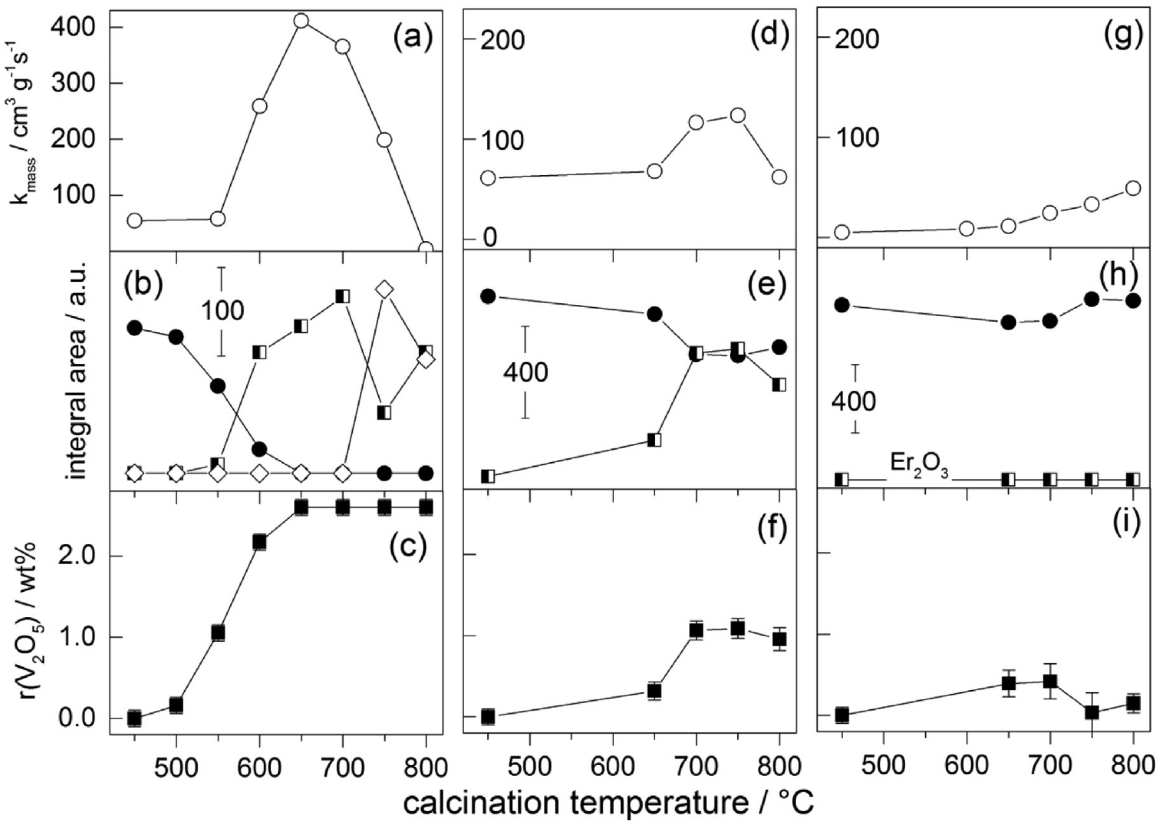

Fig. 5. k_{mass} values obtained at 300 °C for (a) 5FeV-TWS, (d) 9CeV-TWS and (g) 10ErV-TWS calcined at the indicated temperatures. (b) XRD peak integral areas of 5FeV-TWS (● $FeVO_4$, 27.2°; ◧ Fe_2O_3, 33.1°; ◇ Fe_2WO_6, 31.0°, data from Fig. S4). (e) XRD peak integral areas of 9CeV-TWS (● $CeVO_4$, 32.4°; ◧ CeO_2, 28.6°). (h) XRD peak integral areas of 10ErV-TWS (● $ErVO_4$, 33.6°; ◧ Er_2O_3, 29.3°, data from Fig. S5). (c,f,i) Corresponding estimated released fractions of V_2O_5 ($r(V_2O_5)$).

revealed that decomposition of supported $CeVO_4$ started between 650 °C and 700 °C. The catalytic activity (k_{mass}) passed through a maximum value after calcination at 750 °C, which matched with the maximum of CeO_2 formation. The increase in $r(V_2O_5)$, which is responsible for the SCR reaction on V_2O_5-based catalysts [3], also became measurable after calcination at 700 °C and increased continuously with increasing calcination temperature. The k_{mass} value of 6CeV-TWS-750 °C (79 cm^3 g^{-1} s^{-1}, Table 1) was between those of 0.5V-TWS (67 cm^3 g^{-1} s^{-1}, Table 2) and 1V-TWS (148 cm^3 g^{-1} s^{-1}) and the NO reduction efficiency was intermediate between those of the two V_2O_5-based catalysts (Fig. 2b). Accordingly, $r(V_2O_5)$ of 6CeV-TWS-750 °C (ca. 0.7 wt%) was intermediate between the nominal V_2O_5 loadings of 0.5V-TWS and 1V-TWS. Therefore, the activity of 6CeV-TWS was closely related to the evolution of SCR-active VO_x species and to the decomposition of $CeVO_4$. In Fig. 5, the catalysts with the highest NO reduction efficiency for each metal vanadate, namely 5FeV-TWS (Fig. 5a–c), 9CeV-TWS (Fig. 5d–f) and 10ErV-TWS (Fig. 5g–i) were compared with each other with respect to k_{mass}, the relevant XRD peak integrals and the estimated $r(V_2O_5)$ for each composition. The k_{mass} of the fresh catalysts was rather modest. Similar to Fig. 4, calcination at higher temperature produced increasingly active catalysts which is evident at 600 °C for 5FeV-TWS (Fig. 5a), at 700 °C for 9CeV-TWS (Fig. 5d) and only limited above 700 °C for 10ErV-TWS (Fig. 5g). Moreover, the activity of 5FeV-TWS and 9CeV-TWS decreased sharply after calcination at 700 °C and 800 °C, respectively. The integrals of selected XRD reflections of the corresponding vanadate and oxide phases closely followed this behavior (Fig. 5b, e and h). The decrease of the $FeVO_4$ reflection and the appearance of Fe_2O_3 (Fig. 5b) started to be noticeable at around the same temperature as the change in k_{mass}. $FeVO_4$ vanished completely above 650 °C. Fe_2O_3 still slightly increased after calcination at 700 °C before passing through a minimum at 750 °C that was concomitant to the appearance and decomposition of Fe_2WO_6. This observation suggests that iron released from $FeVO_4$ decomposition reacted with WO_3 of TWS. The formation of Fe_2WO_6 above 650 °C is plausible because a metastable α-Fe_2WO_6 can form at 650–750 °C [41]. 9CeV-TWS progressed similarly exhibiting an increase of CeO_2 content and a decrease of $CeVO_4$ after calcination at 700 °C. Complete disappearance of the $CeVO_4$ phase never occurred and the extent of decomposition did not change considerably above 700 °C. Finally, in marked contrast to FeV-WTS and CeV-TWS, the $ErVO_4$ phase in 10ErV-TWS remained almost unperturbed at all calcination temperatures and no Er_2O_3 could be detected by XRD (Fig. 5h). The data of Fig. 5 indicates that the supported metal vanadates underwent decomposition to different extents. The propensity to decomposition was in the order $FeVO_4$ > $CeVO_4$ > $ErVO_4$ and followed the stability order of the unsupported counterparts, $FeVO_4$ < $CeVO_4$ < $ErVO_4$ [5,6,42]. $FeVO_4$ is the least stable vanadate and decomposes consistently at lower temperature once it is supported on TWS.

The decomposition of supported $FeVO_4$ and $CeVO_4$ generated the corresponding single oxides and free VO_x species on the catalyst. The estimated amounts of $r(V_2O_5)$ are displayed in Fig. 5c, f and i for 5FeV-TWS, 9CeV-TWS and 10ErV-TWS, respectively. It is remarkable that, similar to 6CeV-TWS (Fig. 4), the changes of $r(V_2O_5)$ and k_{mass} are closely correlated. Fig. 5c demonstrates that complete $FeVO_4$ decomposition into VO_x and oxide/tungstate species occurred after calcination above 600 °C. 5FeV-TWS was the most active SCR catalyst in the series shown in this work and exhibited the largest fraction of released VO_x. A remaining vanadate phase was detected at all calcination temperatures in 9CeV-TWS and 10ErV-TWS and the maximum $r(V_2O_5)$ was ca. 1.1 wt% and

0.4 wt%, respectively. As a consequence, 9CeV-TWS exhibited moderate SCR activity above the calcination temperature of 700 °C. The SCR activity of this sample matched that of 1V-TWS (Fig. 2b), a strong evidence for the direct correlation between $r(V_2O_5)$ and NO reduction efficiency for this type of catalysts. To this end, 10ErV-TWS barely showed any SCR activity in agreement with the negligible value of $r(V_2O_5)$. Therefore, the poor reactivity of ErV-TWS catalysts can be attributed to the high thermal stability of $ErVO_4$ and to its inability to decompose on TWS (Fig. S5). The three metal vanadate-based catalysts exhibited improved SCR activity only after calcination at temperatures where the vanadate phases decomposed.

The decomposition of the vanadates also affected the thermal stability of the catalysts. 5FeV-TWS, which displayed the largest fraction of released V_2O_5, experienced the largest extent of phase transition from anatase to rutile after calcination at 800 °C (Fig. S4), followed by 9CeV-TWS and 10ErV-TWS. The extent of sintering of the support is thus dependent on the amount of VO_x that is made available from decomposition of the vanadate, in agreement with the role of vanadium in promoting the phase transition of TiO_2 in SCR catalysts [3,4,43]. The lower the temperature of vanadate decomposition, the earlier TWS sintered.

It has to be mentioned that the V content of 5FeV-TWS (2.7 wt% V_2O_5) was lower compared to that of 9CeV-TWS (3.3 wt% V_2O_5) and 10ErV-TWS (3.3 wt% V_2O_5). The 5 wt% $FeVO_4$ loading of 5FeV-TWS was selected based on its optimal performance and after the consideration that a high loading accelerates the sintering of the support [31]. In this respect, FeV-TWS with a $FeVO_4$ loading equivalent to the 3.3 wt% V_2O_5 of 9CeV-TWS and ErV-TWS would cause severe aging already at moderate calcination temperatures. The effect of sintering was already evident in the XRD patterns (Fig. S4) and in the decreasing k_{mass} values (Fig. 5a) of 5FeV-TWS calcined at 700–800 °C.

Compared to 5FeV-TWS, $r(V_2O_5)$ of 9CeV-TWS and 10ErV-TWS was lower at all calcination temperatures (Fig. 5c, f and i, respectively) and the TWS support was not affected by sintering or by phase transitions. This is also evident by comparison of the k_{mass} values after calcination at 750 °C in Tables 1 and 2. CeV-TWS catalysts exhibited increasing NO reduction efficiency with increasing $CeVO_4$ loading and increasing amount of released $r(V_2O_5)$, which however never exceeded values higher than ca. 1 wt%. Hence, a direct correlation between $r(V_2O_5)$ and SCR activity (k_{mass}) can be obtained only when VO_x species are not yet initiating the TWS sintering.

The vanadates were therefore compared at lower but identical V_2O_5 content ($MeVO_4$ loading corresponding to 2 wt% V_2O_5, Fig. S6) and the same set of experiments was conducted as in Fig. 5. This guaranteed a retarded sintering of the support and thus a more careful comparison. Although small differences in the onset of temperature of decomposition and formation of metal oxides were found, the correlation between catalytic activity and $r(V_2O_5)$ remained valid. The increase in NO reduction efficiency upon calcination can be conclusively linked to the partial or complete decomposition of the metal vanadates into single metal oxides and VO_x species. Despite the activation through calcination at high temperature, the rare earth metal based catalysts were not as active as conventional V_2O_5-based catalysts because only a fraction of the metal vanadate decomposed. Reference catalysts with the similar V_2O_5 loading as the $r(V_2O_5)$ of $MeVO_4$ demonstrated the validity of the correlation between activity and $r(V_2O_5)$. It has to be mentioned that the correlation was not anymore valid after severe aging of the catalyst at 800 °C. While the $MeVO_4$ decomposition still occured, the catalyst started sintering (phase transformation of TiO_2 and crystallite growth of WO_3, Fig. 3) and the surface area decreased, factor that are responsible for the drop in the catalytic activity. This phenomenon was initiated at lower calcination temperature with increasing V content.

The selection of an alternative source of $CeVO_4$ may represent an option to improve the performance of a vanadate-based catalyst. $CeVO_4$ used to produce the CeV-TWS series so far was pre-treated at 700 °C and was thus already a crystalline material (crystallite size: 80 ± 1 nm according to XRD, Fig. 3). The pre-treatment of $CeVO_4$ was beneficial for the characterization of the catalysts by XRD because the $CeVO_4$ reflections were clearly visible. However, the initial physico-chemical properties of the material may influence the NO reduction efficiency. Smaller crystallites (14 ± 2 nm, Table S1) were measured when $CeVO_4$ was only dried after precipitation from the Ce and V precursors. A catalyst identical to 6CeV-TWS was then prepared with 5.6 wt% of dried $CeVO_4$ (6CeV-dried-TWS, 2.0 wt% V_2O_5). The behavior of this material (Fig. S6j–l) in terms of changes in phase composition with increasing calcination temperature was similar to that of 6CeV-TWS (Fig. S6d–f, see also Fig. 4). The $r(V_2O_5)$ value (calculated from data in Fig. S7) and k_{mass} increased with increasing temperature, while $CeVO_4$ progressively decomposed to CeO_2, but 6CeV-dried-TWS exhibited twofold values of k_{mass} and $r(V_2O_5)$ (174 $cm^3\ g^{-1}\ s^{-1}$ and 1.5 wt%) compared to 6CeV-TWS (79 $cm^3\ g^{-1}\ s^{-1}$ and 0.7 wt%). Therefore, around twice as much $CeVO_4$ decomposed in the case of 6CeV-dried-TWS in agreement with the twofold increase in NO reduction efficiency. Moreover, the highest k_{mass} of CeV-dried-TWS was obtained already after calcination at 650 °C, i.e. 100 °C lower than in the case of CeV-TWS (750 °C), which was accompanied by aging effects after calcination at 800 °C. Based on the above observations on the various vanadate catalysts, we can conclude that the higher activity at lower calcination temperature was caused by an easier $CeVO_4$ decomposition as a result of the smaller particle size and the partially amorphous state of $CeVO_4$. However, this also implies that deactivation occurred at lower temperature and that it was caused by an early and accelerated sintering induced by the free VO_x species according to the mechanisms known for V_2O_5-based catalysts. Hence, small $MeVO_4$ particles are beneficial for the activity of vanadate-based catalysts, not because $MeVO_4$ is more active but because the onset of its decomposition is shifted to lower temperature.

3.2.2. BET surface area and surface coverage of V

The BET surface area of the catalysts (Tables 1 and 2) provided precious information about the sintering of the support material and was a crucial parameter to estimate the V surface coverage. The surface area of TWS (78 m^2/g) decreased with increasing V content to 72 m^2/g (0.5V-TWS), 61 m^2/g (1V-TWS) and to 21 m^2/g (2V-TWS) after calcination at 750 °C, thus reflecting the influence of V content on the stability of the support material [3]. It decreased only slightly up to 1 wt% V_2O_5, indicating that TWS withstands calcination at 750 °C within a certain threshold of V content. In contrast, the surface area of the CeV-TWS catalysts did not change up to 9 wt% $CeVO_4$ (ca. 70 m^2/g) after calcination at 750 °C, while it decreased to 53 m^2/g in the case of 11CeV-TWS, presumably because $r(V_2O_5)$ exceeded 1 wt% (Table 1). This is also evident in the case of FeV-TWS, where the surface area dropped below 50 m^2/g in both materials used in this study.

The nominal V surface coverage (ξ) was calculated from the BET surface area assuming a theoretical value of 7.9 $VO_x\ nm^{-2}$ for a monolayer coverage (Tables 1 and 2) [44]. We recently showed that ideal V_2O_5-WO_3-TiO_2 catalysts in terms of activity and stability possess ξ values comprised between 25 and 50% [3]. Below 25%, the V content is too low and/or the surface area too high accounting for their modest catalytic activity but also for their resistance to thermal aging. Higher NO reduction efficiency can be achieved by increasing the loading of the active phase or by decreasing the surface area upon increasing the calcination temperature. However, the stability of the catalyst is not guaranteed above ξ = 50% and the

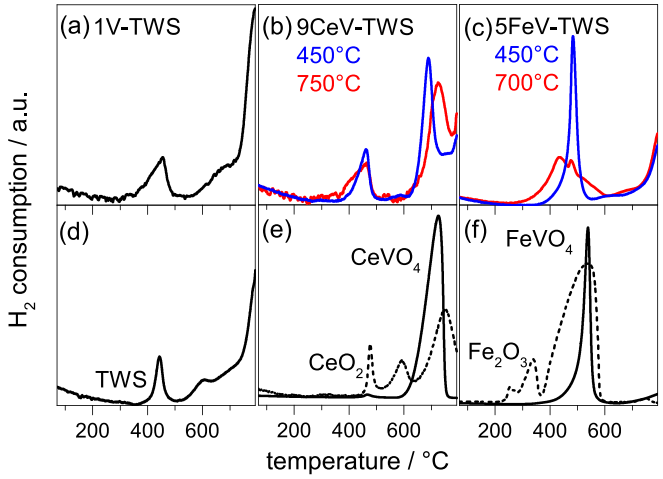

Fig. 6. H_2-TPR profiles of (a–c) selected SCR catalysts and (d–f) corresponding reference materials.

NO reduction efficiency decreases after exposure to high calcination temperature. This argument holds also for the V-TWS catalysts of this work.

0.5V-TWS and 1V-TWS displayed ξ values of 6% and 14%, respectively (Table 2). By increasing the V content to 2 wt% (2V-TWS) and the calcination temperature to 750 °C, ξ increased to 80% and the sintering of TWS was evident in XRD (Fig. S3). Table 1 demonstrates that the estimated ξ values of all CeV-TWS and ErV-TWS catalysts were never above 20% after calcination at 750 °C thus matching the low activity levels of these catalysts. The increase in $CeVO_4$ loading resulted in higher ξ because of the increasing $r(V_2O_5)$ value. This was also the fate of 5FeV-TWS (ξ = 69%) because of the complete decomposition of $FeVO_4$. On the contrary, the value of ξ obtained for 4FeV-TWS was within the 25 and 50% range (34%) and lead to the highest k_{mass} value among all the catalysts after calcination at 750 °C (Tables 1 and 2).

3.2.3. H_2-TPR

The surface redox properties of selected catalysts were characterized by temperature-programmed reduction by hydrogen (H_2-TPR, Fig. 6). While XRD cannot deliver evidence for the presence of VO_x species, H_2-TPR is sensitive to reduction of V^{5+} species irrespective of their crystallinity degree. This is demonstrated in Fig. 6a and d for 1V-TWS. The symmetric H_2 consumption peak of TWS at ca. 440 °C (Fig. 6d) corresponding to the $W^{6+} \rightarrow W^{4+}$ reduction broadened towards low temperature (380–460 °C) because of the overlap with the $V^{5+} \rightarrow V^{3+}$ reduction [45] in 1V-TWS (Fig. 6a). Further reduction events at ca. 600 and 800 °C belong to complete reduction of the WO_3 component [46]. Unsupported $CeVO_4$ (Fig. 6e) and $FeVO_4$ (Fig. 6f) reduced in a single event at 725 °C and 540 °C, respectively demonstrating the ease of reducibility of the latter vanadate. These reduction events shifted to lower temperature in fresh 9CeV-TWS (Fig. 6b) and fresh 5FeV-TWS (Fig. 6c) as a result of the presence of TWS, while the reduction peak of WO_3 was evident only in 9CeV-TWS. The H_2-TPR profiles changed significantly upon calcination at 750 °C. The thermogram of 9CeV-TWS is complex and presents two H_2 consumption events at 460 °C and 725 °C. The latter reduction peak may be associated with the reduction of $CeVO_4$, the XRD data of Fig. 3 however showed that only a portion of $CeVO_4$ survived calcination at 750 °C. Comparison with the H_2-TPR of CeO_2 reveals that the high temperature reduction needs to be associated to reduction of both the remaining $CeVO_4$ and the CeO_2 [47] produced upon $CeVO_4$ decomposition. The increased H_2 consumption at ca. 400 °C is attributed to reduction of the corresponding fraction of VO_x species released from decomposed $CeVO_4$ at 750 °C.

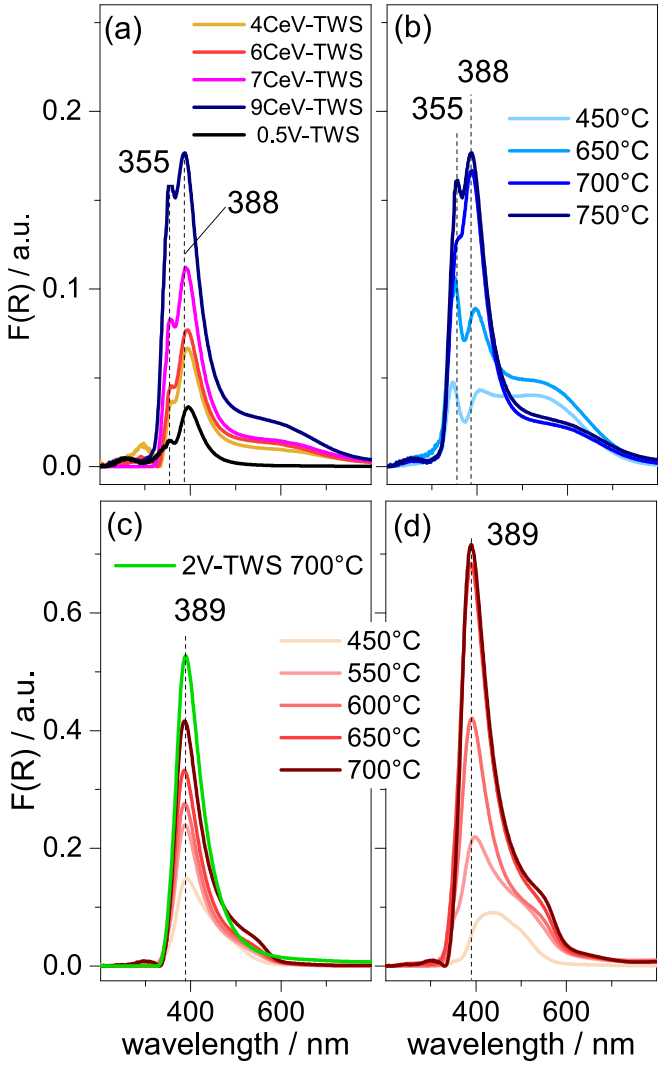

Fig. 7. Diffuse reflectance UV–vis spectra of (a) CeV-TWS and 0.5V-TWS calcined at 750 °C, (b) 9CeV-TWS, (c) 4FeV-TWS (and 2V-TWS) and (d) 5FeV-TWS calcined at various temperatures.

While $CeVO_4$ was still partly available in CeV-TWS, $FeVO_4$ decomposition was extensive in 5FeV-TWS calcined at 700 °C (Fig. 6c). The sharp reduction peak of bulk $FeVO_4$ was replaced almost completely by a broad feature at 300–600 °C after calcination at 700 °C that we assign to the simultaneous reduction of Fe and V oxides formed upon $FeVO_4$ decomposition and of W^{6+} in TWS. The remarkable difference between the two thermograms of 5FeV-TWS clearly suggests that $FeVO_4$ present in the fresh sample disappears after calcination above 700 °C, in agreement with the data of Fig. 5.

3.2.4. Diffuse reflectance UV–vis spectroscopy

In order to verify the presence of VO_x species from decomposition of the supported metal vanadates, diffuse reflectance UV–vis (DRUV) spectra of CeV-TWS (Figs. 7 a and 6 b), FeV-TWS (Fig. 7c and d) and ErV-TWS (Fig. S12) were recorded and TWS background corrected (Fig. S8). Despite the awareness of the impact of drying the samples prior to spectroscopic investigations [48], we found no substantial difference between the spectra of selected ambient and dehydrated samples (Fig. S9) and analyzed the catalysts without drying. The spectra in Fig. 7 were dominated by a signal at ca. 388 nm that was accompanied by a weaker and broad feature extending to ca. 700 nm. In the case of CeV-TWS and 0.5V-TWS, a second sharp signal at 355 nm was also present. The 355

and 388 nm signals intensified not only with increasing $CeVO_4$ loading (Fig. 7a) but also with increasing calcination temperature (Fig. 7b). While it could be argued from Fig. 7a that the stronger absorbance is a loading effect, Fig. 7b gives a clear indication that these two features derive from increasing amounts of VO_x species. An increase in the calcination temperature of 9CeV-TWS promoted $CeVO_4$ decomposition into CeO_2 and VO_x species (Fig. 5). Because CeO_2 mainly absorbs below 300 nm (Fig. S10a), the signals between 300 and 400 nm were assigned to signatures of VO_x species. The increased intensity of these two signals with increasing $CeVO_4$ loading (Fig. 7a) is the result of an increased amount of released vanadium (Table 1). Identical features between 300 and 400 nm were also found in 0.5V-TWS (Fig. 7a), indicating that similar VO_x species to those obtained from $CeVO_4$ decomposition cover the TWS surface.

In the case of 5FeV-TWS (Fig. 7d) only one main feature at 389 nm was visible above a calcination temperature of 550 °C in correspondence to the $FeVO_4$ decomposition occurring at around this temperature. This feature was not visible in the fresh state, supporting the findings that $FeVO_4$ did not decompose at this temperature (Fig. 5b) [31]. The spectra did not change significantly after calcination at 700 °C, suggesting that no further change occurred in the VO_x population. This is in agreement with the observation that at this temperature supported $FeVO_4$ mostly decomposed to Fe_2O_3 (Figs. 5b and 7c) and that $r(V_2O_5)$ remained constant at the maximum value (Fig. 5c). After calcination above 650 °C, 5FeV-TWS showed stronger signals compared to those of 4FeV-TWS (Fig. 7c) as a consequence of the higher $r(V_2O_5)$ value at the equivalent temperatures.

The decomposition of the supported metal vanadates could also be followed by DRUV. The signature of bulk $CeVO_4$ in Fig. 7b was centered at ca. 550 nm extending to 700 nm (see also Figs. S10 and S11a). This signal attenuated steadily with increasing calcination temperature but never disappeared suggesting that a fraction of $CeVO_4$ survived above 700 °C in agreement with the trends observed in the XRD data. The same signal increased with increasing $CeVO_4$ loading after calcination at 750 °C suggesting that the remaining fraction of $CeVO_4$ was proportional to the $CeVO_4$ loading (Fig. 7a). A similar behavior was observed also for the FeV-TWS catalysts (Fig. 7c and d). $FeVO_4$, identified by the broad absorption from 400 to 500 nm, was only visible in fresh FeV-TWS (Fig. S11b). By increasing the calcination temperature, a feature at ca. 525 nm appeared and intensified that was assigned to the growth of the Fe_2O_3 phase (Figs. S10a and S11d) in agreement with the XRD results. No major spectral changes were found for ErV-TWS (Fig. S12) between calcination at 450 °C and at 750 °C. The low intensity of the signal appearing at ca. 400 nm compared to CeV-TWS catalysts further verified the findings from XRD that only small amounts of VO_x species were released for 10ErV-TWS.

A more detailed assignment of the features observed in the DRUV spectra to specific VO_x species is not straightforward. The available literature is ambiguous on the nuclearity of the VO_x species. For the purpose of our discussion and according to the trends visible in the spectra presented, we refer to VO_x species organized in small and large domains to avoid speculations. It is evident from the presented spectra that with higher V_2O_5 loading (e.g. 2V-TWS) or large $r(V_2O_5)$ (FeV-TWS, Fig. 7c and d), only the 389 nm feature was detected. Because the calculated VO_x surface coverage was higher for 2V-TWS and FeV-TWS compared to CeV-TWS samples (Tables 1 and 2), we conclude that the 389 nm feature could origin from extended domains of VO_x. This is further strengthened by the attribution of a transition at ca. 400 nm to polymerized VO_5/VO_6 species on SiO_2 in both ambient and dehydrated conditions [49,50] and to polymeric distorted tetrahedral VO_4 units on TiO_2 [51,52]. The DRUV spectrum of 0.5V-TWS-750 in Fig. 7a exhibited a similar signal at 389 nm but of lower intensity because of the lower equivalent V content of 0.5V-TWS than in all CeV-TWS catalysts. It can also be assumed that the impregnation of TWS to obtain 0.5V-TWS produced a better V_2O_5 dispersion thus leading to a lower extent of agglomeration. The contribution of the VO_x species in the large domains increased upon increasing the calcination temperature of 9CeV-TWS (Fig. 7b), 4FeV-TWS (Fig. 7c) and 5FeV-TWS (Fig. 7d), suggesting that the released fraction of VO_x from decomposition of the metal vanadate produced a high degree of polymerization.

The signal at 355 nm was present only in catalysts with low $r(V_2O_5)$ (CeV-TWS, affording between 0.5 and 1.1 wt% V_2O_5, Table 1) and in 0.5V-TWS (Fig. 7a). It is therefore plausible that this feature origins from small VO_x domains. Also the reference materials $Zn_3(VO_4)_2$ or Na_3VO_4 (isolated monomeric tetrahedral units; 349 and 352 nm, respectively) and $Ba_2V_2O_7$ or $Sr_2V_2O_7$ (dimeric tetrahedral units; 336 and 343 nm, respectively) exhibited a similar $O \rightarrow V^{5+}$ charge transfer transition [53,54]. The V_2O_5 loading was linked to the presence of this transition: the signal vanished by increasing the V_2O_5 loading to 2 wt% (2V-TWS, Fig. 7c) indicating that all VO_x units agglomerated to form the domains characterized by the signal at 388 nm. The transition from small to large VO_x domains at higher V_2O_5 loading can also be followed during the decomposition of supported $FeVO_4$. The shoulder at 355 nm was still visible in the spectrum of 5FeV-TWS calcined at 550 °C (Fig. 7d), suggesting a partial population of small VO_x domains. This is reasonable because the estimated $r(V_2O_5)$ was ca. 1.0 wt% (Fig. 5c). At higher calcination temperature, $FeVO_4$ decomposed completely into Fe_2O_3 and VO_x, thus increasing the surface VO_x concentration and causing the disappearance of the signal at 355 nm at lower calcination temperature than in the case of CeV-TWS.

Finally, the low energy shoulder in the DRUV spectra of FeV-TWS indicates an additional feature that was isolated by fitting the spectra using a signal at ca. 400–450 nm (Fig. S11). This signal was attributed to bulk-like V_2O_5 species [52] that were most prominent in 2V-TWS-700 and 5FeV-TWS-700. The same feature was also observed in 9CeV-TWS and indicates that the VO_x species represented by the peak at 389 nm further aggregated to a bulk-like V_2O_5 phase of amorphous character since they remain XRD invisible. Only 0.5V-TWS exhibited high energy signatures that was assigned to isolated species (Fig. 7a) [50,55]. The synthesis method used to prepare V-TWS (impregnation with ammonium metavanadate) is probably beneficial to obtain more uniformly distributed VO_x species.

3.2.5. NH_3 ADSORPTION

Diffuse reflectance infrared Fourier transformed (DRIFT) spectra of adsorbed NH_3 on CeV-TWS, 1V-TWS and TWS were recorded in order to probe directly the VO_x and WO_x species. For this purpose, the spectral region of the overtones of the stretch modes of vanadyl (V=O) and tungstenyl (W=O) groups at 2050–2000 cm^{-1} is represented in Fig. 8. The relative intensity of these signals can also deliver information on changes of W and V surface coverage (Table S2) [56]. Additional spectral features are described in Fig. S13. It should be noted here that no NH_3 adsorbed on $CeVO_4$. Because of the strong overlap of signals associated with both functional groups perturbed by NH_3 adsorption (Fig. S13), the 2100–1950 cm^{-1} spectral region of 6CeV-TWS, 9CeV-TWS, 1V-TWS and TWS was background corrected, normalized and deconvoluted (Fig. 8). This exercise clearly evidenced 2ν(W=O) features at ca. 2000–2020 cm^{-1} [56] for all samples and 2ν(V=O) features at ca. 2030–2055 cm^{-1} [57] in the vanadium containing catalysts (Fig. 8c–h). A feature was found at ca. 2050 cm^{-1} (VO_A) in the fresh catalyst and after calcination at 750 °C. A second component (VO_B) at ca. 2035 cm^{-1} (fresh state) and 2040 cm^{-1} (after calcination at 750 °C) was necessary to fit the spectra satisfactorily. Association of the different degrees of nuclearity of VO_x and the correspond-

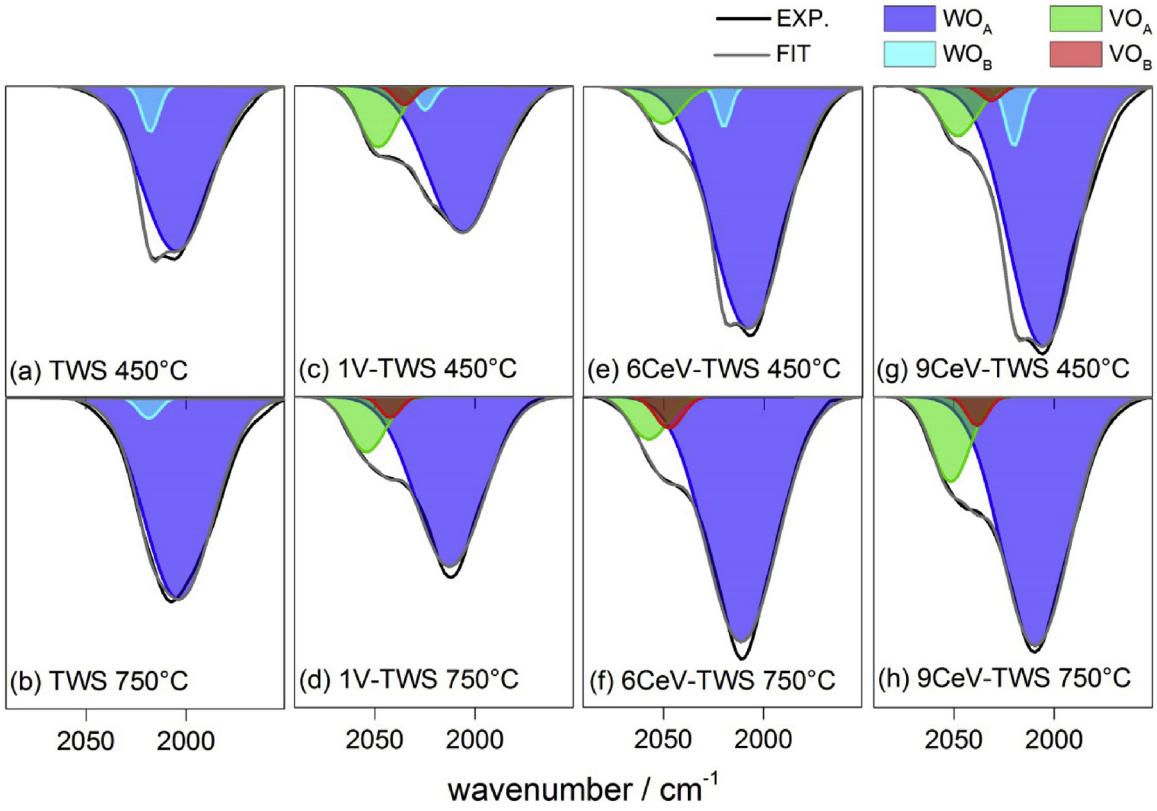

Fig. 8. Deconvoluted DRIFT spectra of in the 2ν(W=O) and 2ν(V=O) overtone region of selected catalysts. Spectra were obtained after adsorption of NH_3 at 250 °C.

ing energy shifts is rather ambiguous in the available literature [49,58–62], making the assessment of the precise nature of these signals difficult. The present data reveals that already the fresh CeV-TWS catalyst exhibit a limited amount of free VO_x species which were possibly formed during the washcoat procedure. It can therefore be assumed that intrinsic activity of the fresh CeV-TWS catalysts in Fig. 1 origin from small amounts of VO_x species. The DRIFTS data further showed that calcination at 750 °C did not affect the V=O signals of 1V-TWS (Fig. 8c–d) because the VO_x content does not change and the support sintering was not initiated. However, the intensity of the V=O features in 9CeV-TWS increased from 9% to 18% relative to the WO_B signal after calcination at 750 °C (Fig. 8g–h, Table S2). This observation agrees well with the increase in $r(V_2O_5)$, the increased value of k_{mass} (Fig. 5) and the increased VO_x absorption signals in the DRUV spectra (Fig. 7) and confirms the presence of an increased amount of VO_x species with increasing calcination temperature. The same accounts for 6CeV-TWS (Fig. 8e and f), but the V=O contribution increased only from 10% to 12%. Since 6CeV- and 9CeV-TWS do not show any aging tendency at 750 °C (same TiO_2 crystallite sizes and BET surface area, Table 1) and did not exhibit any crystalline V- or W-containing phase in the XRD (Fig. S3), we conclude that the larger V=O contribution in 9CeV-TWS is related to the correspondingly higher $r(V_2O_5)$ values of Table 1. It is further notable that an identical fraction of VO_x species was estimated for 1V-TWS and 9CeV-TWS after calcination at 750 °C (Table S2), in agreement with the calculated $r(V_2O_5)$ for 9CeV-TWS (1.1 wt%) and the V_2O_5 loading in 1V-TWS (1.0 wt%). The VO_B component was of lower intensity for both catalysts than VO_A. Identical to VO_A, VO_B intensified after calcination of 9CeV-TWS at 750 °C but remained similar in the case of 1V-TWS. We tentatively assign this signal to vanadyl species of limited nuclearity, similar to our conclusion from the DRUV data.

Finally, the deconvolution of 1V-TWS, 9CeV-TWS and TWS confirmed that the fresh samples comprised two tungstenyl species with 2ν(W=O) at ca. 2010 cm^{-1} (WO_A) and ca. 2020 cm^{-1} (WO_B), which were both perturbed by NH_3 addition (Fig. 8a, c and e). These two features remained unchanged in TWS after calcination at 750 °C (Fig. 8f). However, the WO_B signal disappeared in the CeV-TWS and 1V-TWS spectra, possibly due to the presence of VO_x units covering the mentioned tungstenyl species. This assumption is strengthened by the fact that fresh 1V-TWS exhibited a lower fraction of WO_B due to the larger V_2O_5 content compared to fresh 9CeV-TWS.

The diffuse reflectance spectroscopy experiments unambiguously unveiled the presence of VO_x species from decomposed $MeVO_4$. They were therefore an essential complement to the XRD and H_2-TPR data, where the formation of VO_x species could only be followed indirectly.

4. Conclusions

The nature of active species and the dependence of calcination temperature of $CeVO_4$, $FeVO_4$ and $ErVO_4$ catalysts on SiO_2-WO_3-TiO_2 were investigated. It was shown that the catalysts became more active after the metal vanadate started to decompose into metal oxides and freed VO_x species. While the $FeVO_4$-based catalyst completely decomposed into Fe_2O_3 and VO_x species, the rare earth metal based catalysts only decomposed partially which could be directly correlated to their lower activity but high stability. This correlation could be verified by preparing vanadia-based catalysts of similar loading as the amount of released VO_x species from the metal vanadate, which resulted in identical activity and stability. The limited decomposition of the rare earth metal vanadates generated low levels of released VO_x species dispersed on the support, which in turn was responsible for the high temperature stability of the catalysts. The decomposition and consequently the activity of $MeVO_4$ based catalysts could be improved using vanadates of lower crystallinity, which however accelerated the aging of the

catalyst. It was shown that a released fraction of ca. 1 wt% V_2O_5 is sufficient to induce catalyst aging at a calcination temperature above 750 °C. The evidence of the presence of released VO_x species was obtained from H_2-TPR, DRUV and DRIFT spectroscopy. Similar vanadyl species to those of vanadia-based catalysts were found. At elevated calcination temperature, VO_x migrates towards WO_3 surface species which is a potential initiation step for the sintering of the support material. The decomposed metal vanadates predominantly form extended VO_x domains while the impregnated vanadia-based catalysts feature also VO_x domains of lower nuclearity. Due to the generation of VO_x species at elevated temperatures, $MeVO_4$ could be envisaged as precursor materials for active phases for various reaction catalyzed by vanadium.

Acknowledgements

The authors gratefully acknowledge the financial support of Treibacher Industrie AG and the Austrian Research Promotion Agency (FFG, framework Frontrunner). Ms. C. Erismann is acknowledged for the assistance with the catalytic activity measurements and Mr. S. P. Steiger for the H_2-TPR measurements. The work was conducted in the framework of the SCCER BIOSWEET program.

Appendix A. Supplementary data

Supplementary data associated with this article can be found, in the online version, at http://dx.doi.org/10.1016/j.apcatb.2017.06.061.

References

[1] P. Forzatti, Present status and perspectives in de-NOx SCR catalysis, Appl. Catal. A: Gen. 222 (2001) 221–236.
[2] M. Koebel, M. Elsener, M. Kleemann, Urea-SCR: a promising technique to reduce NOx emissions from automotive diesel engines, Catal. Today 59 (2000) 335–345.
[3] A. Marberger, M. Elsener, D. Ferri, O. Kröcher, VOx surface coverage optimization of V2O5/WO3-TiO2 SCR catalysts by variation of the V loading and by aging, Catalysts 5 (2015) 1704–1720.
[4] G. Madia, M. Elsener, M. Koebel, F. Raimondi, A. Wokaun, Thermal stability of vanadia-tungsta-titania catalysts in the SCR process, Appl. Catal. B: Environ. 39 (2002) 181–190.
[5] J. Walczak, I. Rychłowska-Himmel, Phase diagram of the FeVO4·Fe2WO6 system, Thermochim. Acta 239 (1994) 269–274.
[6] V. Panchal, S. López-Moreno, D. Santamaría-Pérez, D. Errandonea, F.J. Manjón, P. Rodríguez-Hernandez, A. Muñoz, S.N. Achary, A.K. Tyagi, Zircon to monazite phase transition in CeVO4: X-ray diffraction and Raman-scattering measurements, Phys. Rev. B 84 (2011) 024111.
[7] M. Casanova, K. Schermanz, J. Llorca, A. Trovarelli, Improved high temperature stability of NH3-SCR catalysts based on rare earth vanadates supported on TiO2/WO3/SiO2, Catal. Today 184 (2012) 227–236.
[8] M. Casanova, E. Rocchini, A. Trovarelli, K. Schermanz, I. Begsteiger, High-temperature stability of V2O5/TiO2-WO3-SiO2 SCR catalysts modified with rare-earths, J. Alloys Compd. 408–412 (2006) 1108–1112.
[9] Y. Pan, W. Zhao, Q. Zhong, W. Cai, H. Li, Promotional effect of Si-doped V2O5/TiO2 for selective catalytic reduction of NOx by NH3, J. Environ. Sci. (China) 25 (2013) 1703–1711.
[10] X. Liu, X. Wu, T. Xu, D. Weng, Z. Si, R. Ran, Effects of silica additive on the NH3-SCR activity and thermal stability of a V2O5/WO3-TiO2 catalyst, Chin. J. Catal. 37 (2016) 1340–1346.
[11] D. Chapman, G. Fu, S. Augustine, J.e.a. Crouse, New titania materials with improved stability and activity for vanadia-based selective catalytic reduction of NOx, SAE Int. J. Fuels Lubr. 3 (2010) 643–653.
[12] D.A.H. Hanaor, C.C. Sorrell, Review of the anatase to rutile phase transformation, J. Mater. Sci. 46 (2011) 855–874.
[13] M. Casanova, J. Llorca, A. Sagar, K. Schermanz, A. Trovarelli, Mixed iron–erbium vanadate NH3-SCR catalysts, Catal. Today 241 (Part A) (2015) 159–168.
[14] K.A. Michalow-Mauke, Y. Lu, K. Kowalski, T. Graule, M. Nachtegaal, O. Kröcher, D. Ferri, Flame-made WO3/CeOx-TiO2 catalysts for selective catalytic reduction of NOx by NH3, ACS Catal. 5 (2015) 5657–5672.
[15] F. Liu, Y. Yu, H. He, Environmentally-benign catalysts for the selective catalytic reduction of NOx from diesel engines: structure-activity relationship and reaction mechanism aspects, Chem. Commun. 50 (2014) 8445–8463.
[16] W. Shan, F. Liu, Y. Yu, H. He, The use of ceria for the selective catalytic reduction of NOx with NH3, Chin. J. Catal. 35 (2014) 1251–1259.
[17] X. Wang, L. Zhang, S. Wu, W. Zou, S. Yu, Y. Shao, L. Dong, Promotional effect of Ce on iron-based catalysts for selective catalytic reduction of NO with NH3, Catalysts 6 (2016) 112.
[18] L. Chen, J. Li, M. Ge, Promotional effect of Ce-doped V2O5-WO3/TiO2 with low vanadium loadings for selective catalytic reduction of NOx by NH3, J. Phys. Chem. C 113 (2009) 21177–21184.
[19] C. Li, Q. Li, P. Lu, H. Cui, G. Zeng, Characterization and performance of V2O5/CeO2 for NH3-SCR of NO at low temperatures, Front. Environ. Sci. Eng. 6 (2012) 156–161.
[20] L. Chen, Z. Si, X. Wu, D. Weng, R. Ran, J. Yu, Rare earth containing catalysts for selective catalytic reduction of NOx with ammonia: a review, J. Rare Earths 32 (2014) 907–917.
[21] X. Zhao, L. Huang, S. Namuangruk, H. Hu, X. Hu, L. Shi, D. Zhang, Morphology-dependent performance of Zr-CeVO4/TiO2 for selective catalytic reduction of NO with NH3, Catal. Sci. Technol. 6 (2016) 5543–5553.
[22] M.A.L. Vargas, M. Casanova, A. Trovarelli, G. Busca, An IR study of thermally stable V2O5-WO3 -TiO2 SCR catalysts modified with silica and rare-earths (Ce, Tb, Er), Appl. Catal. B: Environ. 75 (2007) 303–311.
[23] S. Gillot, J.P. Dacquin, C. Dujardin, P. Granger, High intrinsic catalytic activity of CeVO4-based catalysts for ammonia-SCR: influence of pH during hydrothermal synthesis, Top. Catal. 59 (2016) 987–995.
[24] X. Zhao, L. Huang, H. Li, H. Hu, X. Hu, L. Shi, D. Zhang, Promotional effects of zirconium doped CeVO4 for the low-temperature selective catalytic reduction of NOx with NH3, Appl. Catal. B: Environ. 183 (2016) 269–281.
[25] L. Huang, X. Zhao, L. Zhang, L. Shi, J. Zhang, D. Zhang, Large-scale growth of hierarchical transition-metal vanadate nanosheets on metal meshes as monolith catalysts for De-NOx reaction, Nanoscale 7 (2015) 2743–2749.
[26] M. Casanova, L. Nodari, A. Sagar, K. Schermanz, A. Trovarelli, Preparation, characterization and NH3–SCR activity of FeVO4 supported on TiO2–WO3–SiO2, Appl. Catal. B: Environ. 176–177 (2015) 699–708.
[27] M. Casanova, A. Sagar, K. Schermanz, A. Trovarelli, Enhanced stability of Fe2O3-doped FeVO4/TiO2–WO3–SiO2 SCR catalysts, Top. Catal. 59 (2016) 996–1001.
[28] P. Zhang, D. Li, Selective catalytic reduction of NO with NH3 over iron–vanadium mixed oxide catalyst, Catal. Lett. 144 (2014) 959–963.
[29] G. Wu, J. Li, Z. Fang, L. Lan, R. Wang, M. Gong, Y. Chen, FeVO4 nanorods supported TiO2 as a superior catalyst for NH3–SCR reaction in a broad temperature range, Catal. Commun. 64 (2015) 75–79.
[30] F. Liu, H. He, Z. Lian, W. Shan, L. Xie, K. Asakura, W. Yang, H. Deng, Highly dispersed iron vanadate catalyst supported on TiO2 for the selective catalytic reduction of NOx with NH3, J. Catal. 307 (2013) 340–351.
[31] A. Marberger, M. Elsener, D. Ferri, A. Sagar, K. Schermanz, O. Kröcher, Generation of NH3 selective catalytic reduction active catalysts from decomposition of supported FeVO4, ACS Catal. 5 (2015) 4180–4188.
[32] M. Kleemann, M. Elsener, M. Koebel, A. Wokaun, Investigation of the ammonia adsorption on monolithic SCR catalysts by transient response analysis, Appl. Catal. B: Environ. 27 (2000) 231–242.
[33] O. Kröcher, M. Devadas, M. Elsener, A. Wokaun, N. Söger, M. Pfeifer, Y. Demel, L. Mussmann, Investigation of the selective catalytic reduction of NO by NH3 on Fe-ZSM5 monolith catalysts, Appl. Catal. B: Environ. 66 (2006) 208–216.
[34] M. Koebel, M. Elsener, G. Madia, Recent Advances in the Development of Urea-SCR for Automotive Application, SAE Technical Paper, 2001 (N. 2001-2001-3625).
[35] M. Casapu, O. Kröcher, M. Elsener, Screening of doped MnOx–CeO2 catalysts for low-temperature NO-SCR, Appl. Catal. B: Environ. 88 (2009) 413–419.
[36] M. Koebel, M. Elsener, Selective catalytic reduction of NO over commercial DeNOx-catalysts: experimental determination of kinetic and thermodynamic parameters, Chem. Eng. Sci. 53 (1998) 657–669.
[37] S. Djerad, L. Tifouti, M. Crocoll, W. Weisweiler, Effect of vanadia and tungsten loadings on the physical and chemical characteristics of V2O5-WO3/TiO2 catalysts, J. Mol. Catal. A-Chem. 208 (2004) 257–265.
[38] P. Kubelka, F. Munk, Ein Beitrag zur Optik der Farbanstriche, Z. Tech. Phys. 12 (1931) 593–601.
[39] M. Wojdyr, Fityk: a general-purpose peak fitting program, J. Appl. Crystallogr. 43 (2010) 1126–1128.
[40] D.M. Chapman, Behavior of titania-supported vanadia and tungsta SCR catalysts at high temperatures in reactant streams: tungsten and vanadium oxide and hydroxide vapor pressure reduction by surficial stabilization, Appl. Catal. A: Gen. 392 (2011) 143–150.
[41] J. Walczak, I. Rychiowska-Himmel, P. Tabero, Iron(III) tungstate and its modifications, J. Mater. Sci. 27 (1992) 3680–3684.
[42] J.R. Gambino, C.J. Guare, Yttrium and rare earth vanadates, Nature 198 (1963) 1084.
[43] G.C. Bond, A.J. Sárkány, G.D. Parfitt, The vanadium pentoxide-titanium dioxide system: structural investigation and activity for the oxidation of butadiene, J. Catal. 57 (1979) 476–493.
[44] I.E. Wachs, Raman and IR studies of surface metal oxide species on oxide supports: supported metal oxide catalysts, Catal. Today 27 (1996) 437–455.
[45] P.G.W.A. Kompio, A. Brückner, F. Hipler, G. Auer, E. Löffler, W. Grünert, A new view on the relations between tungsten and vanadium in V2O5WO3/TiO2 catalysts for the selective reduction of NO with NH3, J. Catal. 286 (2012) 237–247.
[46] C. Wang, S. Yang, H. Chang, Y. Peng, J. Li, Dispersion of tungsten oxide on SCR performance of V2O5WO3/TiO2: acidity, surface species and catalytic activity, Chem. Eng. J. 225 (2013) 520–527.

[47] Z. Lian, F. Liu, H. He, Effect of preparation methods on the activity of VOx/CeO2 catalysts for the selective catalytic reduction of NOx with NH3, Catal. Sci. Technol. 5 (2015) 389–396.
[48] X. Gao, S.R. Bare, B.M. Weckhuysen, I.E. Wachs, In situ spectroscopic investigation of molecular structures of highly dispersed vanadium oxide on silica under various conditions, J. Phys. Chem. B 102 (1998) 10842–10852.
[49] D. Nitsche, C. Hess, Structure of isolated vanadia and titania: a deep UV Raman, UV–vis, and IR spectroscopic study, J. Phys. Chem. C 120 (2016) 1025–1037.
[50] R. Bulánek, L. Čapek, M. Setnička, P. Čičmanec, DR UV–vis study of the supported vanadium oxide catalysts, J. Phys. Chem. C 115 (2011) 12430–12438.
[51] D.W. Kwon, K.H. Park, S.C. Hong, Effect of vanadium structure and lattice oxygen in V-based TiO2 catalysts on selective catalytic reduction of NOx by NH3, J. Chem. Eng. Jpn. 49 (2016) 526–533.
[52] D. Srinivas, W.F. Hölderich, S. Kujath, M.H. Valkenberg, T. Raja, L. Saikia, R. Hinze, V. Ramaswamy, Active sites in vanadia/titania catalysts for selective aerial oxidation of β-picoline to nicotinic acid, J. Catal. 259 (2008) 165–173.
[53] Y. Matsushima, T. Koide, M. Hiro-Oka, M. Shida, A. Sato, S. Sugiyama, M. Ito, Self-activated vanadate compounds toward realization of rare-earth-free full-color phosphors, J. Am. Ceram. Soc. 98 (2015) 1236–1244.
[54] G. Catana, R.R. Rao, B.M. Weckhuysen, P. Van Der Voort, E. Vansant, R.A. Schoonheydt, Supported vanadium oxide catalysts: quantitative spectroscopy, preferential adsorption of V4+/5+, and Al2O3 coating of zeolite Y, J. Phys. Chem. B 102 (1998) 8005–8012.
[55] Z. Wu, H.-S. Kim, P.C. Stair, S. Rugmini, S.D. Jackson, On the structure of vanadium oxide supported on aluminas: UV and visible Raman spectroscopy, UV-visible diffuse reflectance spectroscopy, and temperature-programmed reduction studies, J. Phys. Chem. B 109 (2005) 2793–2800.
[56] G. Ramis, G. Busca, P. Forzatti, Spectroscopic analysis of titania-tungsta-vanadia de NOxing catalysts, Appl. Catal. B: Environ. 1 (1992) L9–L13.
[57] G. Busca, J.C. Lavalley, Use of overtone bands to monitor the state of the catalyst active phases during infrared studies of adsorption and catalytic reactions, Spectrochim. Acta Part A: Mol. Spectrosc. 42 (1986) 443–445.
[58] M. Baron, H. Abbott, O. Bondarchuk, D. Stacchiola, A. Uhl, S. Shaikhutdinov, H.J. Freund, C. Popa, M.V. Ganduglia-Pirovano, J. Sauer, Resolving the atomic structure of vanadia monolayer catalysts: monomers, trimers, and oligomers on ceria, Angew. Chem. Int. Ed. 48 (2009) 8006–8009.
[59] Y. He, M.E. Ford, M. Zhu, Q. Liu, U. Tumuluri, Z. Wu, I.E. Wachs, Influence of catalyst synthesis method on selective catalytic reduction (SCR) of NO by NH3 with V2O5-WO3/TiO2 catalysts, Appl. Catal. B: Environ. 193 (2016) 141–150.
[60] L. Kiwi-Minsker, D.A. Bulushev, F. Rainone, A. Renken, Implication of the acid–base properties of V/Ti-oxide catalyst in toluene partial oxidation, J. Mol. Catal. A-Chem. 184 (2002) 223–235.
[61] N.Y. Topsøe, J.A. Dumesic, H. Topsøe, Vanadia-titania catalysts for selective catalytic reduction of nitric-oxide by ammonia: I.I. Studies of active sites and formulation of catalytic cycles, J. Catal. 151 (1995) 241–252.
[62] G. Busca, G. Centi, L. Marchetti, F. Trifiro, Chemical and spectroscopic study of the nature of a vanadium oxide monolayer supported on a high-surface-area TiO2 anatase, Langmuir 2 (1986) 568–577.